Efficiency Evaluation of Fully Integrated On-Board EV Battery Chargers With Nine-Phase Machines

Nandor Bodo, Emil Levi, *Fellow, IEEE*, Ivan Subotic, *Member, IEEE*, Jordi Espina, Lee Empringham, *Member, IEEE*, and C. Mark Johnson, *Member, IEEE*

***Abstract*—A fully integrated on-board battery charger for future electric vehicles (EVs) has been recently introduced. It reutilizes all the propulsion components of an EV in charging/vehicle-to-grid (V2G) modes, it does not require any additional components or hardware reconfiguration, and charging/V2G modes are realized with zero electromagnetic torque production. Both fast (three-phase) and slow (single-phase) chargings are possible, with unity power factor operation at the grid side. The solution is based on the use of a triple three-phase machine and a nine-phase inverter/rectifier. This paper reports on the results of efficiency evaluation for the said system. Testing is performed using both a nine-phase induction machine and a nine-phase permanent magnet machine for a range of operating conditions in charging/V2G modes, with both three-phase and single-phase grid connection. Additionally, the impact of converter interleaving on the losses and efficiency is also studied. Losses are separated for different subsystems, thus providing an insight into the importance of optimization of different EV power train components from the efficiency point of view. Promising efficiencies, in the order of 90%, are achieved although none of the system components have been optimized.**

***Index Terms*—Battery chargers, electric vehicles, integrated on-board chargers, multiphase machines.**

I. Introduction

INTEGRATED chargers for EVs were considered more than thirty years ago [1]. However, they became the focus of both academia and industry only recently, due to the introduction of numerous novel topologies. A number of newly developed integrated chargers are capable only of single-phase (slow) charging [2] and they are likely to serve only as a potentially valuable ad-on asset in conjunction with fast three-phase chargers. On the other hand, the majority of the proposed three-phase integrated chargers suffer from the problem of torque production in the machine during charging [3]–[6]. This problem can be conveniently eliminated by utilization of multiphase machines, as shown in [7]–[9].

This paper focuses on the integrated on-board charger that has been recognized as the most promising out of the developed multiphase machine/converter based chargers: the one with the nine-phase machine and nine-phase converter, described in conjunction with three-phase and single-phase charging/V2G modes in [10] and [11], respectively.

The main purpose of the paper is to report on the results of loss and efficiency evaluation of the nine-phase charging/V2G system, with a detailed separation of the losses in various components, which then enables certain conclusions to be drawn with regard to possible ways of minimizing them. In contrast to [10] and [11], in this paper both nine-phase induction and PM machines are considered. Use of the PM machine in addition to an induction machine is an important aspect of this paper, since induction and PM machines are met in the majority of EV powertrains [12].

In contrast to [11], where efficiency was reported for a single operating point of the nine-phase induction machine for single-phase charging/V2G modes (and for a different inverter dc voltage), the results here cover the complete feasible power range of operation in both charging and V2G modes.

As shown by measurement results, the obtained efficiency levels are comparable with the ones reported for independent off-board [13], [14] or on-board chargers [15]–[17]. The efficiencies for the available fast off-board chargers are up to 96% [14]. However, at lower charging rates this value can go down to anything around 50%. The highest reported efficiency found in the literature is 98% in a system that incorporates hybrid resonant converter and a zero voltage switching technique working at 100 kHz in a non-integrated charger [17]. Data for the efficiencies of the integrated on-board chargers are practically impossible to find in literature, so that this paper can be regarded as a pioneering work in this area. The achieved efficiency is typically of the order of 85%–90%, as detailed later on.

It has to be noted that the experimental system was built for the concept demonstration and that various components of the system are hugely mismatched with regard to the power ratings. It can be expected that with properly matched components (and with a more sophisticated design of the dc/dc converter) the achievable efficiency would be higher.

The paper is organized as follows. Section II reviews the architecture of the system and its control for three-phase and

Manuscript received March 15, 2016; revised May 24, 2016; accepted August 9, 2016. Date of publication September 15, 2016; date of current version February 16, 2017. This work was supported by the Engineering and Physical Sciences Research Council National Centre for Power Electronics under Grant EP/K035304/1. Paper no. TEC-00212-2016.

N. Bodo and E. Levi are with the Faculty of Engineering and Technology, Liverpool John Moores University, Liverpool L3 3AF, U.K. (e-mail: n.bodo@ljmu.ac.uk; e.levi@ljmu.ac.uk).

I. Subotic is with the Power Electronic Systems Laboratory, ETH Zürich, Zürich 8092, Switzerland (e-mail: subotic@lem.ee.ethz.ch).

J. Espina, L. Empringham, and C. M. Johnson are with the Power Electronics, Machines and Control Group, The University of Nottingham, Nottingham NG7 2RD, U.K. (e-mail: Jorge.Espina@nottingham.ac.uk; Lee.Empringham@nottingham.ac.uk; Mark.Johnson@nottingham.ac.uk).

Color versions of one or more of the figures in this paper are available online at http://ieeexplore.ieee.org.

Digital Object Identifier 10.1109/TEC.2016.2606657

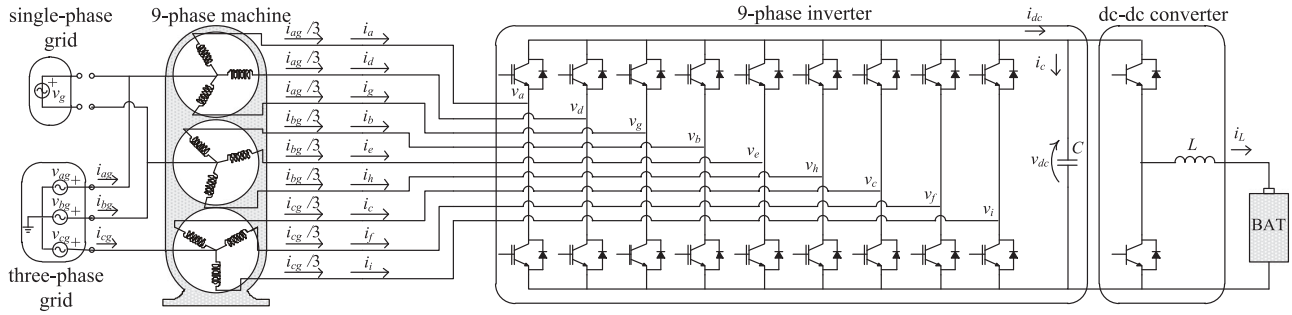

Fig. 1. Topology of the nine-phase fast integrated on-board battery charger in three-phase charging mode.

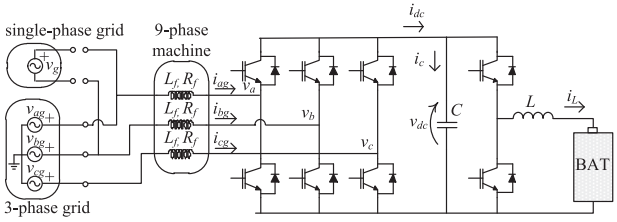

Fig. 2. Equivalent charging/V2G scheme.

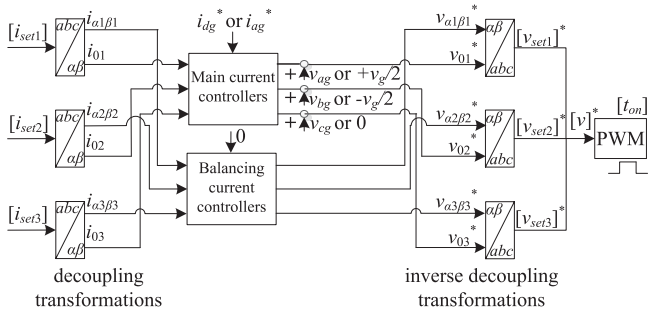

Fig. 3. Control of the converter for three-phase and single-phase grid connection ($i_{dg}{}^*$ is the reference for the d-axis component of the three-phase grid current; $i_{ag}{}^*$ is the grid current reference in single-phase connection).

single-phase charging/V2G operation. Next, the interleaving strategy, which has been considered in [11] for the case of single-phase charging, is reviewed and extended to the three-phase grid connection in Section III. Section IV introduces details of the experimental system and explains the measurement procedure. Loss and efficiency evaluation results are reported in Section V for both nine-phase induction and PM machine, for control with and without interleaving, and for both three-phase and single-phase charging/V2G regimes. Conclusions of the study are given in Section VI.

II. System Description and Control: A Summary

A. System Description

The outlay of the investigated topology is shown in Fig. 1 [10]. During the three-phase charging each grid phase is connected to a separate neutral point of the three three-phase winding sets. Since the individual windings in any three-phase set are displaced by 120° along the stator circumference and the same current flows through each of them, the resulting flux from the individual three-phase sets is zero. If the individual phases of the machine are considered equal, then a simplified equivalent scheme can be used for control purposes. As shown in Fig. 2 the three phases of individual sets can be considered to be connected directly in parallel when the corresponding three inverter legs are switched at the same time. This concept has been explained using nine-phase decoupling matrix transformation and experimentally verified using a nine-phase induction machine in [10].

For the single-phase charging the grid phase and neutral terminals are now connected to two of the three neutral points [11] (Fig. 1). The third set is not used. Once again, the legs connected to the same neutral point are modulated in the same manner and the same currents are drawn through each winding of a three-phase set. Therefore the simplified equivalent scheme is a single-phase full bridge converter (Fig. 2).

B. Control

Grid voltage oriented control is applied for both single-phase and three-phase charging/V2G modes, so that the operation is with unity power factor at the grid side [10], [11]. The control structure (Fig. 3) is briefly addressed next.

During the three-phase charging, the measured currents are passed through a decoupling transformation for each three-phase winding set separately. The resulting zero-sequence currents are then controlled to the desired value via proportional-integral (PI) and resonant vector proportional-integral (VPI) controllers in the 'Main current controllers' (MCCs) block. The MCCs block also contains (only for three-phase charging) a rotational transformation and inverse rotational transformation, to enable current control in a grid-oriented reference frame, so that the fundamental current components appear as dc values.

In the case of single-phase control, only two decoupling transformations are used. The MCCs are placed in the stationary reference frame and only VPI resonant controllers are used.

The outputs of the MCCs are actually the voltage drops on the machine phases. These voltage drops regulate the amount, direction and phase of the current flow to and from the grid. Further, the grid voltages are added to the outputs of the MCCs to enable soft starting of the charging process (v_{ag}, v_{bg} and v_{cg} in three-phase, $+v_g/2$ and $-v_g/2$ in single-phase charging). To minimize noise, these voltages are actually the first harmonics of the grid voltages, extracted through a phase-locked loop [10], [11].

Current control scheme, used in [10], was based on the assumption that all the individual phases of each three-phase winding are identical. However, in practice, some asymmetry

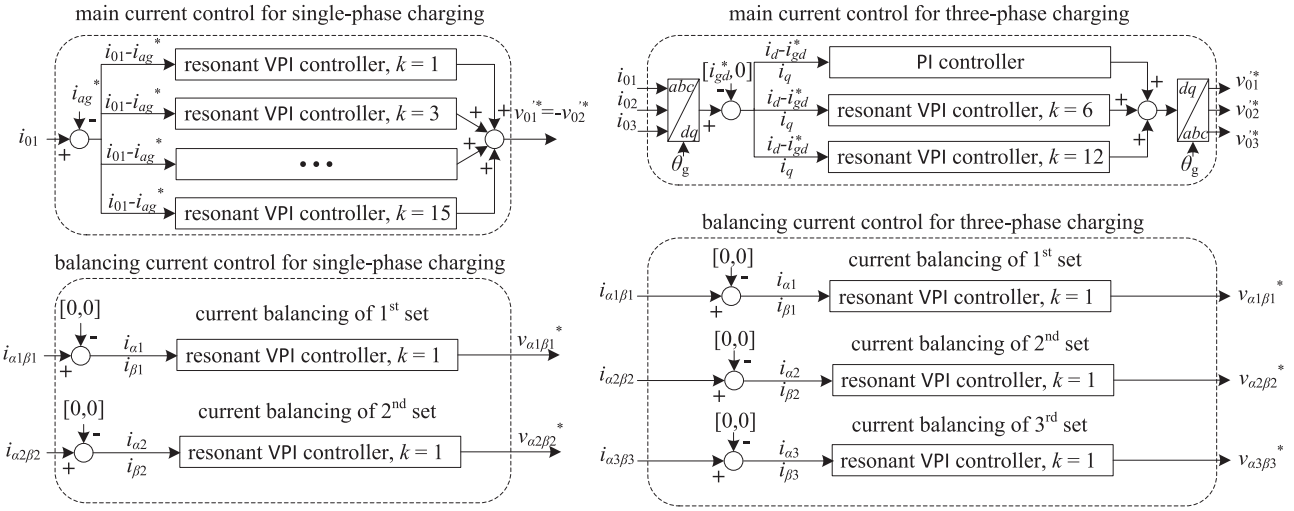

Fig. 4. Current controllers of Fig. 3 for single-phase (left) and three-phase (right) grid connection. MCCs are in the upper part, BCCs are in the lower part.

may appear, leading to imbalance between the currents of the individual phases of the three-phase sets. Therefore, additional current control subsystem is added to the current control structure of [10], to mitigate any possible asymmetry between individual phase windings of the three-phase sets (Fig. 3). The same is done for the single-phase system (Fig. 3).

The α–β components obtained after the initial decoupling transformations, are forwarded to a separate set of 'Balancing current controllers' (BCCs). These control the imbalances between the currents of the individual machine phases of a three-phase set to zero. The BCCs work in the stationary reference frame and contain one resonant VPI controller set to regulate the first harmonic at 50 Hz. In the single-phase charging there are two active BCCs, while in the three-phase charging there are three active BCCs, in accordance with how many three-phase winding sets are used.

The variable k in Fig. 4 defines the harmonic order to which the resonant VPI controllers are tuned to. The BCCs are tuned to the fundamental. In the case of the single-phase grid the MCCs regulate the odd harmonics up to the fifteenth. For three-phase charging the MCCs control the harmonics of the order $1 \pm k$, since the controllers are already placed in the grid oriented reference frame.

Finally, an inverse decoupling transformation combines the efforts of the two sets of current controllers. The resulting voltages are fed to a PWM output block that generates the gating signals for the inverter legs.

In contrast to the studies of [8]–[11], the hardware setup in this paper includes a dc/dc converter, of the simplest bi-directional structure shown in Fig. 1, which is controlled according to the block schematic of Fig. 5. There is an outer control loop controlling the dc-bus voltage at the high voltage (inverter) side. It delivers a reference for the battery charging current i_L. The difference between this reference current and the real battery charging current is then fed to a current controller that outputs the duty cycle for the dc/dc converter. This duty cycle is added

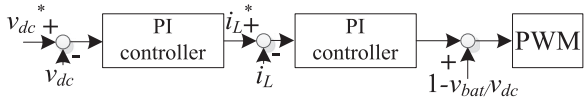

Fig. 5. Control mechanism for the dc/dc converter.

to a feed-forward term that calculates the duty cycle for no-load situation. The resulting on-time is in this case applied to the lower switch in the dc/dc leg depicted in Fig. 1, while the upper switch is commutated in an inverse manner to the lower switch. A detailed analysis and explanations regarding the tuning of such a controller can be found in [18]. The dc/dc converter requires an extra pair of switches (compared to the solution without a dc/dc converter), rated for the full desired charging power.

III. Interleaving Strategy

In order to reduce the grid current ripple, interleaving of the three inverter legs, which are connected to the same neutral point, is considered. This means that the gating signals applied to the three legs are delayed with respect to each other by a third of the switching period. Without interleaving all the components of the machine phase currents are the same in all three legs and they are all transferred to the grid current. When interleaving is applied less ripple is transferred to the grid current. However, some of the machine phase current ripple will inevitably become a circulating current within the three-phase winding, causing additional losses in the machine.

For single-phase charging without interleaving the grid is connected between two neutral points. The three legs on each side of the grid are modulated with the same carrier signals, but with the inverse modulation signal. This results in cancelation of the harmonics that are around the odd multiples of the switching

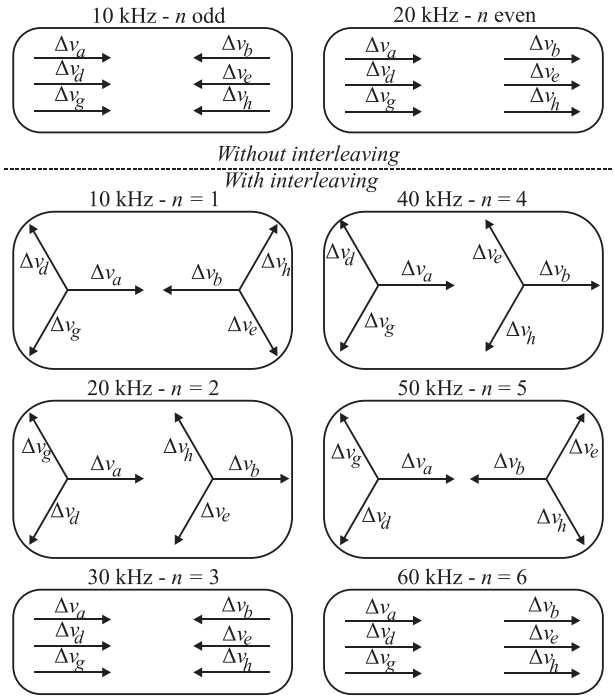

Fig. 6. Switching harmonic positioning around multiples of the switching frequency for single-phase charging.

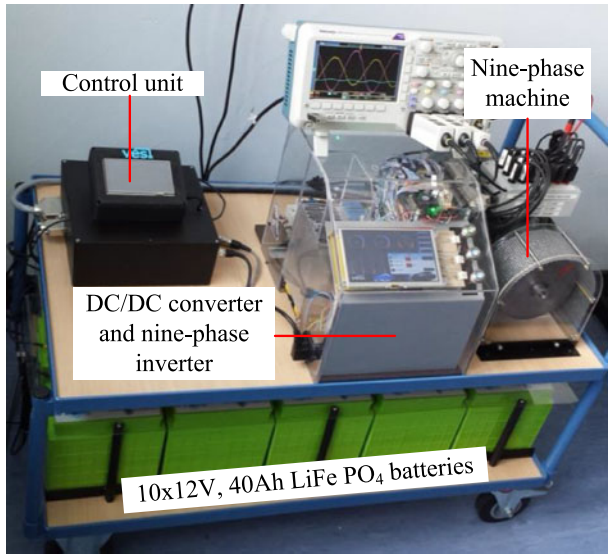

Fig. 7. Physical appearance of the downscaled demonstrator used for obtaining the experimental results (the mounted machine is of induction type).

frequency and doubling of the harmonics that are around even multiples of the switching frequency.

This situation is depicted in Fig. 6, where the switching frequency is taken as 10 kHz (the value used in subsequent experiments). The term Δv indicates voltage ripple of a particular inverter leg, while the encircled voltage ripple groups influence the grid current ripple. The resultant grid current ripple is proportional to the sum of the circled voltage ripple phasors at the indicated frequency.

Once interleaving is applied, the harmonics around the multiples of the switching frequency that were in phase without interleaving, become displaced by $n{\cdot}2\pi/3$, where n is an integer multiplier of the switching frequency. This is also shown in Fig. 6. If $n = 1$, 2, 4 or 5 the harmonics get cancelled within the three interleaved inverter legs individually (phases *a*, *d*, *g* and *b*, *e*, *h*). When $n = 3$, the harmonics of the three legs are actually in phase; however, they cancel with the harmonics from the other three legs, following the reasoning applied for the case without interleaving. It is only for $n = 6$ that some harmonic currents can penetrate the grid. These results were confirmed in simulation. However in experiments the effect of switching of the two three-phase sets is not equal, so that some small harmonics are present at $n = 3$.

It should be noted that the already mentioned efficiency data for a single operating point with single-phase charging topologies in [11] were all obtained without interleaving. The goal here is to evaluate the impact of interleaving on the charging/V2G efficiency across the entire power range.

In the three-phase case, the harmonics at $n = 3$ do not cancel (in contrast to the single-phase case). There is only the effect of interleaving within each set of three-phase windings, eliminating harmonics at $n = 1$, 2, 4 and 5.

IV. Experimental Setup and Measurement Procedure

A. The Experimental Platform

The functionality of the integrated charger/propulsion system has been confirmed experimentally in [10], [11] for three-phase and single-phase charging/V2G operation, using a nine-phase induction machine and a laboratory dc source without a dc/dc converter. For the purposes of this paper a new experimental setup, shown in Fig. 7, has been completed with the inclusion of the dc/dc converter and a battery pack. It can be driven by either a TMS320F28335 controller (indicated in Fig. 7), or by a dSPACE1006 control platform. The latter is selected for the experiments here, for the ease of manipulation. The experimental setup is a stand-alone platform that is capable of operating in: propulsion, propulsion after a fault ('limp-home' mode due to an open-circuit fault; the complete faulty three-phase winding is taken out of operation), single-phase charging/V2G mode, and three-phase charging/V2G mode. The nine-phase induction machine, shown in Fig. 7, can also be replaced with a nine-phase PM machine.

As noted, the switching frequency of the $\mathrm{dc/dc}$ converter and the nine-phase inverter was set to 10 kHz, with asymmetrical PWM. The control loops, therefore, operate twice in each PWM period, at 20 kHz. The battery pack total voltage is around 136 V at no-load conditions, with a separate battery management system taking care of the balancing of the battery state-of-charge on the battery cell level. There is an *LCL* filter between the battery pack and the dc/dc converter (shown just as *L* in Fig. 1 for simplicity), to minimize the adverse effects of the current ripple created by the dc/dc converter on the batteries. The filter parameters are 660 μH (inductance *L* in Fig. 1), 220 μF and 220 μH. The dc/dc converter switches used are Semikron

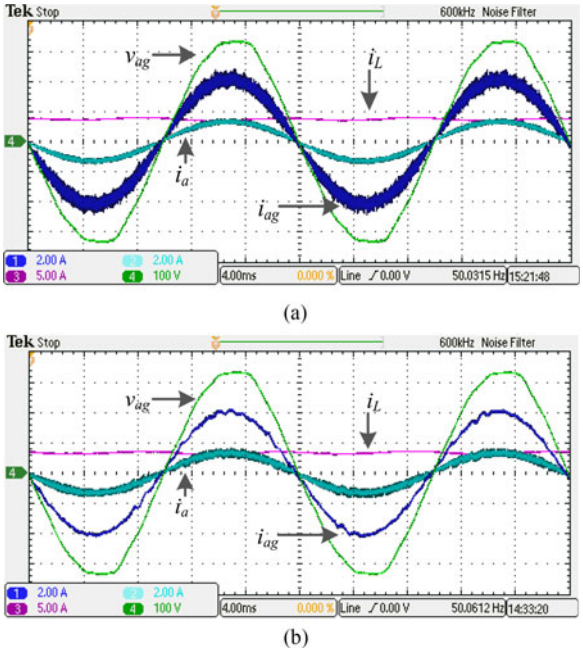

Fig. 8. PM machine, single-phase charging mode: (a) without interleaving, (b) with interleaving (CH1—grid phase current i_{ag}, CH2—machine phase current i_a, CH3—battery charging current i_L, CH4—grid phase voltage v_{ag}).

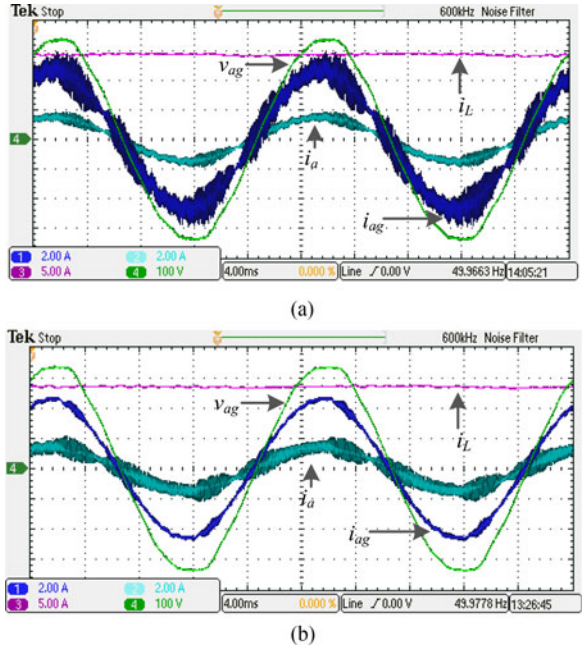

Fig. 9. PM machine, three-phase charging mode: (a) is without interleaving, (b) is with interleaving. Traces as in Fig. 8.

SK100GH12T4T, the total dc-bus capacitance at the inverter dc side is 1162 μF (combination of electrolytic and ceramic capacitors), and the nine-phase inverter switches used are Semikron SK15GD12T4ET. The rated power of the nine-phase inverter is approximately 30 kVA, while the rated power of the dc/dc converter is 7.5 kVA with single half-bridge.

The dc-bus voltage at inverter terminals was controlled to 720 V in three-phase charging/V2G modes and to 450 V in single-phase charging/V2G modes. It should be noted that, although it is possible to perform single-phase charging with the same dc-bus voltage as for the three-phase charging (720 V), this would cause increased grid current ripple. The dead time was set to 1.5 μs in all inverter legs and the dc/dc converter.

B. Single-Phase and Three-Phase Charging Modes

Since charging/V2G modes of operation with an induction machine have been covered in detail in [10], [11] (albeit using a different dc side configuration), only the samples of experimental results are presented here for the PM machine, for the charging mode. System of Fig. 7 is used, with the induction machine replaced by a PM machine.

The charging mode of operation, using single-phase grid, is illustrated in Fig. 8. The oscilloscope recordings are shown with and without interleaving (grid voltage, battery current, grid current and machine current traces are given). Grid current is in essence three times larger than the machine's phase current, in terms of both the fundamental and the ripple. Total harmonic distortion (THD) of both currents is approximately 10%. When interleaving is applied, the grid phase current has a substantially reduced ripple (THD is 2.8%). It can be seen however that the machine's current distortion has increased significantly (THD is 15.6%).

A sample of results for the three-phase charging is shown in Fig. 9, again without and with interleaving. The battery charging current is now free of the second harmonic. Most of the other conclusions remain similar to the ones valid for single-phase charging. The grid phase current has low distortion again, while the machine's phase current has a larger switching ripple than the grid current when interleaving is applied. It is interesting to note that the grid current ripple without interleaving is substantially higher in Fig. 9 than with single-phase charging, Fig. 8. The reason for this is non-cancellation of the switching harmonics (see Section III).

C. Power Measurement Procedure

The powers in the system were measured with a Voltech PM3300 Universal Power Analyzer and the measurements confirmed in several measurement points with a Tektronix MSO2014 oscilloscope. Simultaneous measurements were taken of the power at the battery terminals (using one channel of the instrument) and the grid connections (using the other two channels of the instrument, in two-wattmeter power measurement configuration for three-phase charging; a single channel for single-phase charging) and these determine the total system efficiency. The losses in the machine were also measured, in a separate test with identical input/output system powers, by measuring the power dissipated in the machine (symmetry of three-phase windings of the machines is assumed in these measurements and subsequent calculations).

To be able to separate the dc/dc converter losses from the rest, an additional test was done where a Spitzenberger laboratory dc source was directly connected to the inverter dc side (i.e., batteries and the dc/dc converter are not used in this measurement) and input/output powers were measured as described above. This was necessary since direct power measurement on

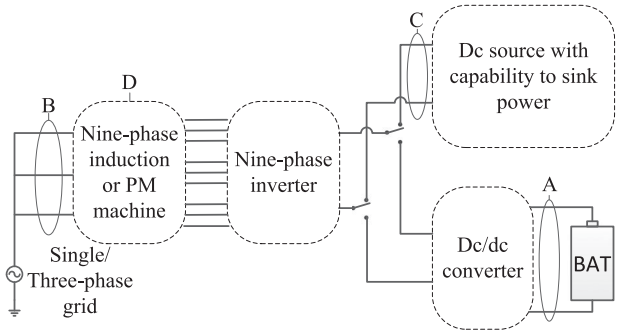

Fig. 10. Power measurement points for loss separation and efficiency evaluation. See Table I for exact definition of each letter in the figure.

TABLE I
DEFINITION OF POWER MEASUREMENT POINTS AND LOSS CURVES IN SUBSEQUENT FIGURES

Fig. 10	Measured power definition
A [W]	Battery power (charging = out, V2G = in)
B [W]	Grid power (charging = input, V2G = output)
C [W]	Spiztenberger power (output/input as in A)
D [W]	Power consumed in the machine
Loss curves	**Obtained using measured powers as**
1, 2, 3 [W]	D
4, 5 [W]	B-C in charging, C-B in V2G mode
6, 7 [W]	B-A in charging, A-B in V2G mode

the high-voltage dc side of the dc/dc converter in Fig. 7 is not physically possible. In these measurements control set points, inverter/rectifier dc side voltage and grid power are kept at the same values as in corresponding measurements with the battery and the dc/dc converter. Fig. 10 illustrates the measurement points in the system that are subsequently used to determine the losses/powers at different system points. The losses and efficiency are plotted against the power drawn from the grid, which is negative in V2G mode and positive in charging operation. Various powers/points shown in Fig. 10 are defined in Table I. Note that the operation on the grid side is always with unity power factor [10], [11].

V. EVALUATION OF LOSSES AND EFFICIENCY

A. Three-Phase Charging/V2G Operation

The three-phase charging is addressed first. The losses encountered in the individual parts of the setup are displayed in Fig. 11 for the induction machine and in Fig. 12 for the PM machine, using the data defined in Fig. 10 and Table I. Traces 1, 2, 3 all illustrate machine losses. The lowest trace (number 1) shows the losses caused by the fundamental components of the currents flowing through the stator windings of the machine. The next trace (number 2) represents the losses inflicted by the total currents flowing through the machine windings, including switching harmonics, for the case without interleaving. If interleaving is applied, the stator current flow leads to more losses, as indicated by the trace number 3, which is above the previous one.

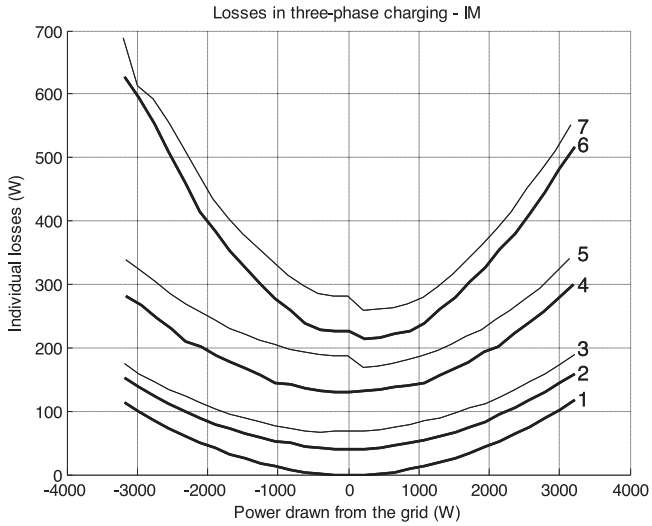

Fig. 11. Induction machine, three-phase grid connection: losses in the machine (1, 2, 3), machine plus converter (4, 5), and total losses including the dc/dc converter (6, 7) with and without interleaving.

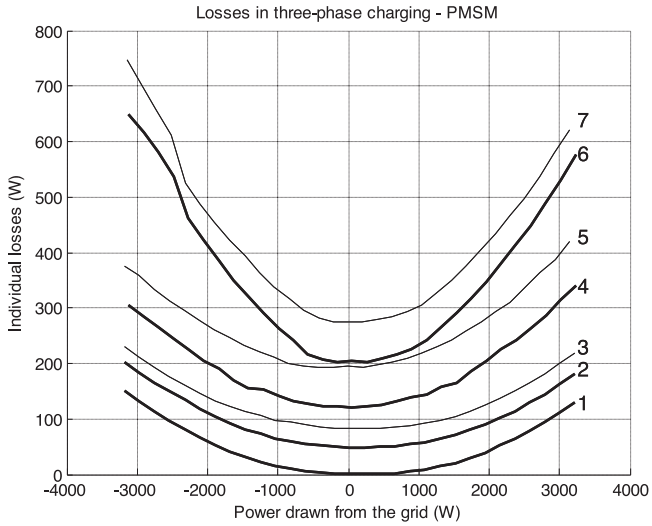

Fig. 12. PM machine, three-phase grid connection: losses in the machine (1, 2, 3), machine plus converter (4, 5), and total losses including the dc/dc converter (6, 7) with and without interleaving.

The second set of two traces (nos. 4 and 5) represents the combined losses of the machine and the nine-phase converter. The lower trace represents the case without interleaving, while the upper one is with interleaving. The difference between the second set of traces 4, 5 and the traces of the first set 2, 3 represents the losses within the nine-phase converter. The uppermost two traces (nos. 6 and 7) show the total losses in the whole system, including the machine, nine-phase converter and the dc/dc converter. Once again, the lower trace shows the case without and the upper one with interleaving. The difference between traces 6 and 4 (7 and 5, respectively) represents the losses within the dc/dc converter.

Fundamental current loss in the machine (trace 1 in Figs. 11–12 and also in corresponding displays of results for single-phase charging) resembles a curve that depends on the

square of the power drawn from (injected into) the grid. This is expected, since the machine current is proportional to the grid power and losses are proportional to the current squared. It can be seen that this loss is slightly higher in the PM machine, due to a higher stator resistance value.

The difference in Figs. 11–12 between the traces 2 and 1, and 3 and 1, respectively, is close to a constant throughout the injected power range, indicating the roughly constant losses caused by the current ripple with and without interleaving. Indeed, the inverter provides voltages with roughly the same magnitude throughout the injected power range, since it has to meet the grid voltage applied to the other side of the stator windings. Only slight alterations of the inverter output voltage cause the control of the current flow, and thus the power injection, by controlling the voltage drop on the machine windings. Consequently, the voltage switching ripple is approximately the same across the whole power range. The filtering of the voltage ripple into the current ripple is governed by the stator leakage inductance of the machine. Indeed, the increment of losses is higher in the case of the PM machine, due to the smaller stator leakage inductance.

The losses due to switching harmonics are around 40 W for the induction machine and 50 W for the PM machine, without interleaving, and around 60 W and 80 W, respectively, for the case with interleaving. Higher switching harmonics of the currents cause higher losses in the inverter as well. The difference between the losses with and without interleaving widens when the inverter losses are also taken into account, to between 35 W and 55 W for the induction machine, and approximately 85 W for the PM machine.

As can be seen, the dc/dc converter causes, when used, a substantial part of the total losses. This is so since a simple bidirectional dc/dc converter topology was used here. A significant reduction of the dc/dc converter losses can be expected if more advanced (e.g. resonant) topologies are used instead. Losses in the dc/dc converter are higher in the V2G mode since in that case the battery acts as a source for the losses in the topology and the power injected into the grid; therefore the dc/dc converter has to conduct higher current. In a well-designed dc/dc converter an efficiency drop of 2–3% can be anticipated (instead of 5–10%, as here).

When comparing the losses in different machines for the same power drawn from the grid, it can be concluded that they are comparable (slightly lower with an induction machine). Hence there is no clear winner in this respect (PM machine is of course more efficient in the propulsion mode).

The measured output/input powers are used to calculate the efficiency and the results are shown in Fig. 13 for the induction machine and Fig. 14 for the PM machine. Curves 1 and 2 show the efficiency of the complete topology (with the dc/dc converter), both with and without interleaving. Traces 3 and 4 show the efficiency of the topology without the dc/dc converter (i.e. using power at point C in Fig. 10 in calculations), once again, with and without interleaving.

The maximal efficiencies achieved (without the dc/dc converter) are around 92% for the induction machine and 91.5% for the PM machine, although these numbers were noted to go

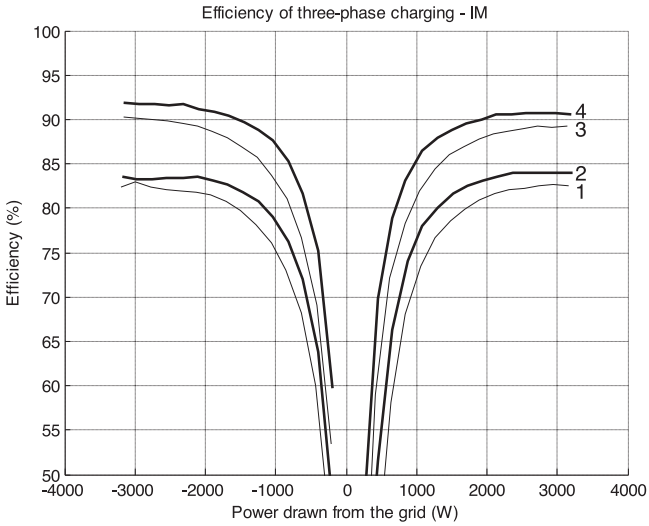

Fig. 13. Induction machine, three-phase charging mode, efficiency: traces 1, 3 are with interleaving, while 2, 4 are without interleaving; traces 1, 2 are with the dc/dc converter, while 3, 4 are without dc/dc converter.

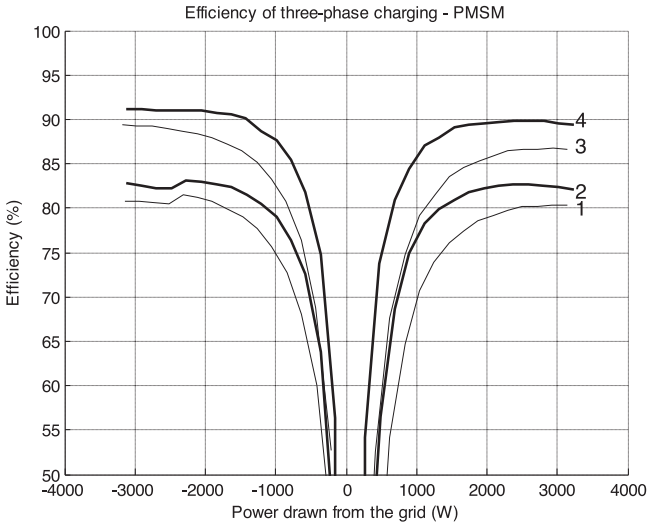

Fig. 14. PM machine, three-phase charging mode, efficiency: traces 1, 3 are with interleaving, while 2, 4 are without interleaving; traces 1, 2 are with the dc/dc converter, while 3, 4 are without dc/dc converter.

up by another 0.5% if the dc-bus voltage is reduced to 700 V. It is also evident that the efficiency is higher in both cases in the V2G mode. This is because the nature of the concept is such that the inverter has to impose lower voltage than the grid voltage in the charging mode, and therefore operates at lower modulation indices, thus not taking advantage of the full dc-bus voltage and leading to the higher switching harmonics. Best performance is therefore achieved if the dc-bus voltage magnitude is controlled so that the inverter works at maximal modulation indices at all instances.

In this case, the efficiencies of 92.5% (induction machine) and 92% (PM machine) can be achieved in the charging mode, as well as in the V2G mode. The dc-bus voltage can be decreased as far down as 600 V at 2.5 kW charging power. This also improves the total efficiency of the topology (when the dc/dc

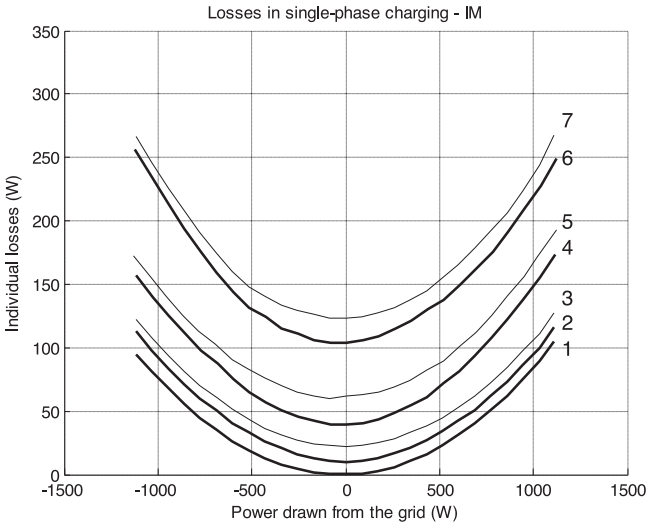

Fig. 15. Induction machine, single-phase grid connection: losses in the machine (1, 2, 3), machine plus converter (4, 5), and total losses including the dc/dc converter (6, 7) with and without interleaving.

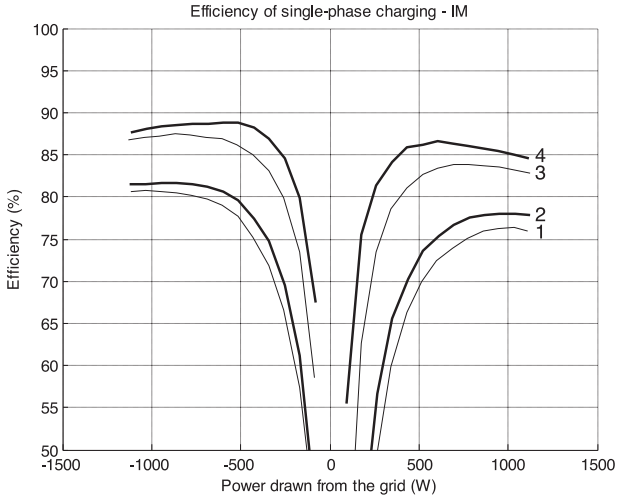

Fig. 16. Induction machine, single-phase charging mode efficiency: traces 1, 3 are with interleaving, while 2, 4 are without interleaving; traces 1, 2 are with the dc/dc converter, while 3, 4 are without dc/dc converter.

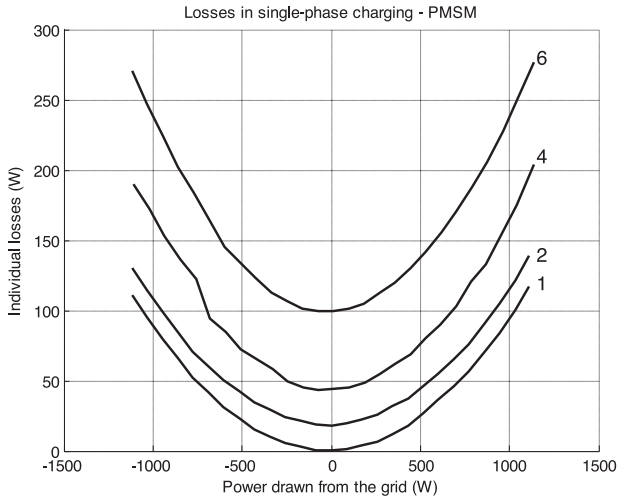

Fig. 17. PM machine, single-phase grid connection: losses in the machine $(1, 2)$, machine plus converter (4), and total losses including the dc/dc converter (6) without interleaving.

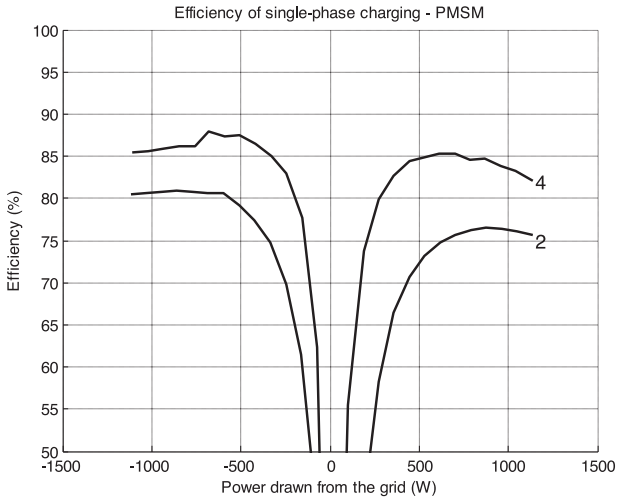

Fig. 18. PM machine, single-phase charging mode, efficiency without interleaving. Trace 4 is without dc/dc converter, trace 2 is with the dc/dc converter.

converter is included) from 84% to about 86% in the case of induction machine and from 82.6% to about 84.4% in the case of PM machine. It therefore appears as justified to use a dc/dc converter, provided that its efficiency is higher than 98% in the charging mode. It is also to be expected that the losses of the dc/dc converter would decrease with an increase of the battery voltage closer to the utilized high dc voltage (720 V).

Applying interleaving might be necessary to comply with the grid code concerning power quality; however, it inevitably decreases the efficiency of the three-phase charging process considerably, by 1.5% to 2%.

B. Single-Phase Charging/V2G Operation

The losses and efficiency for the single-phase charging are shown for the induction machine in Figs. 15 and 16, respectively, both with and without interleaving. Corresponding results for the PM machine are given in Figs. 17 and 18, respectively. However, results with interleaving are now not included, since all the already given results show that the impact of interleaving on efficiency is negative.

The range of the power drawn from (delivered to) the grid is roughly three times smaller compared to the three-phase case. The losses due to the fundamental are six times greater for the same power drawn/delivered compared with the three-phase case because the resistance is in two sets of three-phase windings instead of three and the current is three times larger. The switching losses within the machine are approximately 2.5-3 times lower than in the three-phase case. One would expect that this ratio would be $3/2 = 1.5$ because only two neutrals are used instead of three; however, the single-phase charging has the additional benefit of suppressing the harmonics around the first (without interleaving) or third (with interleaving) multiple of the switching frequency; hence, the switching related loss reduction

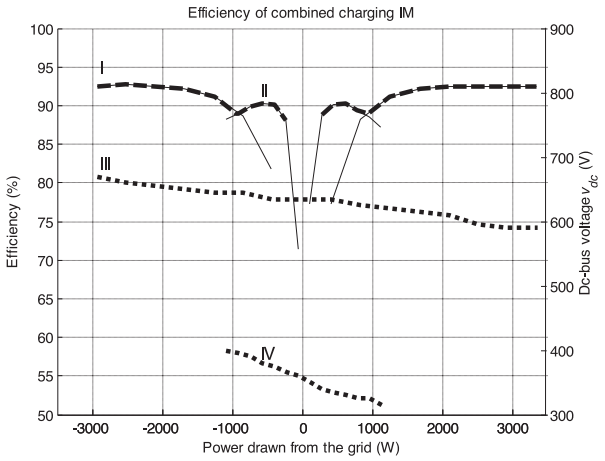

Fig. 19. Induction machine, combined single-phase and three-phase charging: efficiency without interleaving (I— three-phase grid, II—single-phase grid) and applied dc-bus voltage (III—three-phase grid, IV—single-phase grid). Suggested combination of single-phase and three-phase connection for best efficiency performance indicated with bold dashed segments of lines I and II.

is higher. This improvement ratio is kept for the losses within the inverter as well. The losses within the dc/dc converter for the same power delivered to the grid are improved by a ratio of 1.5.

It can be seen that, overall, achieved maximum efficiencies are lower than in the case of three-phase charging. However, in the region of 500 W to 1000 W (in the downscaled prototype used here), the single-phase charging is more efficient.

With regard to the results for the PM machine, given in Figs. 17 and 18, very much the same conclusions apply as for the induction machine. Typically, losses are somewhat higher and hence efficiency slightly lower, primarily due to the higher per-phase stator resistance of the PM machine.

C. Optimal Control Strategy

The optimal control strategy for the nine-phase charger is shown in Fig. 19, where the three-phase charging and single-phase charging are combined to maximize the efficiency. The results in this figure are obtained by decreasing the dc-bus voltage so that the converter works at close to its maximal modulation index at all times. The dc-bus voltage values for the single-phase and three-phase operation are also depicted in Fig. 19 with dotted lines. The bold dashed line shows the proposed combination of the two charging methods by choosing the one with higher efficiency for a given power rate. The application of the system that would enable the changeover from three-phase to single-phase charging would require an additional contactor that would connect the grid neutral instead of the second (or third) grid phase to the second (or third) neutral point of the nine-phase machine.

VI. Conclusion

The fully integrated on-board charger for electrical vehicles, based on a nine-phase converter and electrical machine, is discussed in this paper. The system was tested, using both an induction and a PM machine, in order to evaluate the losses and achievable efficiency. The impact of interleaving, which is advantageous from the point of view of the grid current harmonic content, on the losses and efficiency has also been assessed. The charger losses and efficiency rates, obtained using the described test system, show that the losses in the basic configuration of the dc/dc converter are high and these should be reduced by utilizing a different more advanced topology based on a resonant converter. It is also shown that the application of the interleaving in the nine-phase converter has an adverse effect on the overall efficiency of the charger, creating a need for the trade-off between the grid code requirements and the system efficiency.

Considering that the components of the tested system are mismatched with regard to the power ratings, it is believed that the achieved efficiency rates of the order of 90% are very promising for future investigations of the usability of such a charger in electric vehicles and that higher efficiency rates could be achieved with properly matched components and use of a more sophisticated dc/dc converter.

Appendix

DC sink/source: "Spitzenberger & Spies" – two DM 2500/PAS single-phase mains emulation systems are connected in series. Each provides half of the dc-bus voltage. An additional resistive load (RL 4000) is connected to the supply, to sink up to 4 kW for charging emulation.

Controller: dSPACE DS1006 processor board. A DS2004 high speed A/D board is used for the A/D conversion of the measured machine phase currents and grid voltages. A DS5101 digital waveform output board is used for the PWM signal generation, and the machine speed is read by a DS3002 incremental encoder interface board.

Asymmetrical nine-phase induction machine: The machine was obtained by rewinding the stator of a three-phase machine with rated data 2.2 kW, 230 V (phase-to-neutral), 50 Hz, 4.5 A, $\cos\varphi = 0.83$, two pole pairs, and 36 stator slots. After rewinding, the nine-phase machine is 2.2 kW, 230 V (phase-to-neutral), 50 Hz, and 1.5 A, with one pole pair. The winding layout is available in [10]. Stator per-phase resistance at 50 Hz is measured as 6.8 Ω.

Nine-phase PM machine: The machine was obtained by rewinding the 36-slot stator of a 6-pole three-phase servo surface mounted PM machine with the data: 1.73 kW, 180 V (line-to-line), 150 Hz, 3000 rpm, 5.5 Nm (continuous). After re-winding, the rated per-phase data are 220 V, 1.47 A, 150 Hz. Stator winding is triple-layer, full pitch, with 15° degrees phase shift between first phases of the three-phase windings – the topology is not dependent on phase shift between the three machine sets of windings. Stator per-phase resistance at 50 Hz is measured as 7.9 Ω.

References

[1] J. M. Slicker, "Pulse width modulation inverter with battery charger," U.S. Patent 4 491 768, Jan. 1, 1985.

[2] S. Haghbin, S. Lundmark, M. Alakula, and O. Carlson, "Grid-connected integrated battery chargers in vehicle applications: Review and new solution," *IEEE Trans. Ind. Electron.*, vol. 60, no. 2, pp. 459–473, Feb. 2013.

[3] S. Kinoshita, "Electric system of electric vehicle," U.S. Patent 5 629 603, May 13, 1997.

[4] F. Lacressonniere and B. Cassoret, "Converter used as a battery charger and a motor speed controller in an industrial truck," in *Proc. Eur. Conf. Power Electron. Appl.*, Dresden, Germany, 2005, pp. 1–7.

[5] S. Haghbin, S. Lundmark, M. Alakula, and O. Carlson, "An isolated high-power integrated charger in electrified-vehicle applications," *IEEE Trans. Veh. Technol.*, vol. 60, no. 9, pp. 4115–4126, Nov. 2011.
[6] X. Lu, K. L. V. Iyer, K. Mukherjee, and N. C. Kar, "Investigation of integrated charging and discharging incorporating interior permanent magnet machine with damper bars for electric vehicles," *IEEE Trans. Energy Convers.*, vol. 31, no. 1, pp. 260–269, Mar. 2016.
[7] L. De Sousa, B. Silvestre, and B. Bouchez, "A combined multiphase electric drive and fast battery charger for electric vehicles," in *Proc. IEEE Veh. Power Propulsion Conf.*, Lille, France, 2010, pp. 1–6.
[8] I. Subotic, N. Bodo, and E. Levi, "An EV drive-train with integrated fast charging capability," *IEEE Trans. Power Electron.*, vol. 31, no. 2, pp. 1461–1471, Feb. 2016.
[9] I. Subotic, N. Bodo, E. Levi, M. Jones, and V. Levi, "Isolated chargers for EVs incorporating six-phase machines," *IEEE Trans. Ind. Electron.*, vol. 63, no. 1, pp. 653–664, Jan. 2016.
[10] I. Subotic, N. Bodo, E. Levi, and M. Jones, "Onboard integrated battery charger for EVs using an asymmetrical nine-phase machine," *IEEE Trans. Ind. Electron.*, vol. 62, no. 5, pp. 3285–3295, May 2015.
[11] I. Subotic, N. Bodo, and E. Levi, "Single-phase on-board integrated battery chargers for EVs based on multiphase machines," *IEEE Trans. Power Electron.*, vol. 31, no. 9, pp. 6511–6523, Sep. 2016.
[12] J. de Santiago *et al.*, "Electrical motor drivelines in commercial all-electric vehicles: A review," *IEEE Trans. Veh. Technol.*, vol. 61, no. 2, pp. 475–484, Feb. 2012.
[13] W. Xiaofeng, T. Maeda, H. Fujimoto, S. Ishii, and K. Fujita, "Three-phase high frequency transformer isolated AC to DC converter for EV battery quick charging," in *Proc. Int. Power Electron. Motion Control Conf.*, Harbin, China, 2012, pp. 643–647.
[14] P. Dost, A. Bouabana, and C. Sourkounis, "On analysis of electric vehicles DC-quick-chargers based on the CHAdeMO protocol regarding the connected systems and security behaviour," in *Proc. IEEE Ind. Electron. Soc. Annu. Meet. IECON*, Dallas, TX, USA, 2014, pp. 4492–4497.
[15] K. Obayashi, E. Takahashi, A. Sakamoto, S. Iyasu, S. Ando, and S. Onimaru, "Auxiliary inverter charger (AIC): Concept & experimental results," in *Proc. World Elect. Veh. Symp. Exhib.*, Barcelona, Spain, 2013, pp. 1–6.
[16] L. Mingshuo, C. Qianhong, R. Xiaoyong, Z. Yusheng, J. Ke, and C. Boping, "The integrated LLC resonant converter using center-tapped transformer for on-board EV charger," in *Proc. IEEE Energy Convers. Congr. Expo.*, Montreal, QC, Canada, 2015, pp. 6293–6298.
[17] L. Il-Oun, "Hybrid PWM-resonant converter for electric vehicle on-board battery chargers," *IEEE Trans. Power Electron.*, vol. 31, no. 5, pp. 3639–3649, May 2016.
[18] S. D. Breucker, "Impact of dc-dc converters on Li-ion batteries," Ph.D. dissertation, Katholieke Universiteit Leuven, Leuven, Belgium, 2012.

Nandor Bodo received the Master's degree in power electronics from the Faculty of Technical Sciences, University of Novi Sad, Novi Sad, Serbia, in 2009, and the Ph.D. degree in electrical engineering from Liverpool John Moores University, Liverpool, U.K., in 2013. He is currently with the Liverpool John Moores University, Liverpool, U.K., as a Postdoctoral Research Associate. His research interests include power electronics and variable speed drives.

Emil Levi (S'89–M'92–SM'99–F'09) received the M.Sc. and the Ph.D. degrees in electrical engineering from the University of Belgrade, Belgrade, Yugoslavia, in 1986 and 1990, respectively. In May 1992, he joined Liverpool John Moores University, U.K., where he has been a Professor of electric machines and drives since September 2000. From 2009 to 2013, he was a Coeditor-in-Chief of the IEEE TRANSACTIONS ON INDUSTRIAL ELECTRONICS and is currently an Editor-in-Chief of the *IET Electric Power Applications* and an Editor of the IEEE TRANSACTIONS ON ENERGY CONVERSION. He received the Cyril Veinott Award of the IEEE Power and Energy Society for 2009 and the Best Paper Award of the IEEE TRANSACTIONS ON INDUSTRIAL ELECTRONICS for 2008. In 2014, he received the "Outstanding Achievement Award" from the European Power Electronics Association.

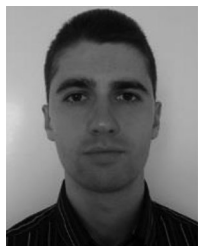

Ivan Subotic (S'12–M'16) received the Dipl.Ing. and the M.Sc. degrees in electrical engineering from the University of Belgrade, Belgrade, Serbia, in 2010 and 2011, respectively, and the Ph.D. degree from Liverpool John Moores University, Liverpool, U.K., in September 2015. He is currently a Postdoctoral Research Associate at ETH Zurich. His research interests include power electronics, electric vehicles, and control of multiphase drive systems.

Jordi Espina received the M.Eng. and Ph.D. degrees from the Universitat Politècnica de Catalunya, Barcelona, Spain, in 2005 and 2011, respectively. He is currently a Research Fellow in the Power Electronics, Machines and Control Group, The University of Nottingham, Nottingham, U.K. His research interests include variable-speed drive systems, EMC, power electronics converters, and integration on power electronics.

Lee Empringham (M'10) received the B.Eng. (Hons.) degree in electrical and electronic engineering and the Ph.D. degree from The University of Nottingham, Nottingham, U.K., in 1996 and 2000, respectively. Since then, he has been with the Power Electronics, Machines and Control Group as a Research Fellow to support different ongoing matrix converter projects and has been recently appointed to the position of Principal Research Fellow. His research interests include direct ac–ac power conversion, variable-speed ac motor drives using different circuit topologies, and more electric/electric aircraft applications. He is a Member of The Institution of Engineering and Technology, U.K.

C. Mark Johnson (M'90) received the B.A. degree in engineering and the Ph.D. degree in electrical engineering from the University of Cambridge, Cambridge, U.K., in 1986 and 1991, respectively. From 1998 to 2001, he managed the U.K. National Programme on Silicon Carbide Electronics. In 2003, he was appointed as a Rolls-Royce/RAEng Research Professor of power electronic systems at The University of Sheffield, Sheffield, U.K., and in 2006, he was appointed as a Personal Chair at The University of Nottingham, Nottingham, U.K. He is the Director of the Centre for Power Electronics of the Engineering and Physical Sciences Research Council of the U.K. and is a Member of the Executive team for the U.K. Innovative Electronics Manufacturing Research Centre.